chemosensors

MDPI

Article

Paper-Based Analytical Devices Based on Amino-MOFs (MIL-125, UiO-66, and MIL-101) as Platforms towards Fluorescence Biodetection Applications

Sofía V. Piguillem [1], Germán E. Gomez [2,*], Gonzalo R. Tortella [3,4], Amedea B. Seabra [5], Matías D. Regiart [6], Germán A. Messina [6] and Martín A. Fernández-Baldo [6,*]

[1] Instituto de Investigaciones en Físico-Química de Córdoba (INFIQC), Departamento de Físico-Química, Universidad Nacional de Córdoba, CONICET, Haya de la Torre Esquina Medina Allende S/N, Córdoba 5000, Argentina; svpiguillem@unsl.edu.ar
[2] Instituto de Investigaciones en Tecnología Química (INTEQUI), Departamento de Química, Universidad Nacional de San Luis (UNSL), CONICET, Ejército de los Andes 950, San Luis D5700BWS, Argentina
[3] Centro de Excelencia en Investigación Biotecnológica Aplicada al Medio Ambiente (CIBAMA), Facultad de Ingeniería y Ciencias, Universidad de La Frontera, Av. Francisco Salazar 01145, Temuco 4811230, Chile; gonzalo.tortella@ufrontera.cl
[4] Departamento de Ingeniería Química, Facultad de Ingeniería y Ciencias, Universidad de La Frontera, Av. Francisco Salazar 01145, Temuco 4811230, Chile
[5] Center for Natural and Human Sciences, Federal University of ABC (UFABC), Avenida dos Estados, Saint Andrew 09210-580, Brazil; amedea.seabra@ufabc.edu.br
[6] Instituto de Química de San Luis, Facultad de Química, Universidad Nacional de San Luis, INQUISAL (UNSL—CONICET), Ejército de los Andes 950, San Luis D5700BWS, Argentina; mregiart@unsl.edu.ar (M.D.R.); messina@unsl.edu.ar (G.A.M.)
* Correspondence: gegomez@unsl.edu.ar (G.E.G.); mbaldo@unsl.edu.ar (M.A.F.-B.)

Abstract: In this study, we designed three promising platforms based on metal–organic frameworks (MOFs) to develop paper-based analytical devices (PADs) for biosensing applications. PADs have become increasingly popular in field sensing in recent years due to their portability, low cost, simplicity, efficiency, fast detection capability, excellent sensitivity, and selectivity. In addition, MOFs are excellent choices for developing highly sensitive and selective sensors due their versatility for functionalizing, structural stability, and capability to adsorb and desorb specific molecules by reversible interactions. These materials also offer the possibility to modify their structure and properties, making them highly versatile and adaptable to different environments and sensing needs. In this research, we synthesized and characterized three different amino-functionalized MOFs: UiO-66-NH_2 (Zr), MIL-125-NH_2 (Ti), and MIL-101-NH_2 (Fe). These MOFs were used to fabricate PADs capable of sensitive and portable monitoring of alkaline phosphatase (ALP) enzyme activity by laser-induced fluorescence (LIF). Overall, amino-derivated MOF platforms demonstrate significant potential for integration into biosensor PADs, offering key properties that enhance their performance and applicability in analytical chemistry and diagnostics.

Keywords: analytical device; paper biosensor; MOFs platform; biomolecules; alkaline phosphatase enzyme

check for updates

Citation: Piguillem, S.V.; Gomez, G.E.; Tortella, G.R.; Seabra, A.B.; Regiart, M.D.; Messina, G.A.; Fernández-Baldo, M.A. Paper-Based Analytical Devices Based on Amino-MOFs (MIL-125, UiO-66, and MIL-101) as Platforms towards Fluorescence Biodetection Applications. *Chemosensors* **2024**, *12*, 208. https://doi.org/chemosensors12100208

Received: 28 August 2024
Revised: 2 October 2024
Accepted: 8 October 2024
Published: 11 October 2024

Copyright: © 2024 by the authors. Licensee MDPI, Basel, Switzerland. This article is an open access article distributed under the terms and conditions of the Creative Commons Attribution (CC BY) license (https://creativecommons.org/licenses/by/4.0/).

1. Introduction

Metal–organic frameworks (MOFs) are attractive crystalline materials made of metal ions or clusters coordinated by multifunctional organic ligands via robust chemical bonds and supramolecular interactions. These assemblies create periodic polymeric networks with organic and inorganic components, spanning two or three dimensions [1]. Moreover, MOF functionalization without altering their structure could be achieved by post-synthesis modifications, allowing unique properties by improving their reactivities [2]. In recent years, MOFs have experienced exponential growth, showing potential applications in

diverse fields such as gas adsorption/separation, controlled drug release, catalysis, and luminescence. This progress allows the rational design of materials with tailored electrochemical and optical properties based on carefully selecting and combining metals and ligands. In general, the properties of MOFs are intimately linked to their structural features, encompassing compositions and architectures [3].

Biochemical analysis often involves lengthy procedures and large, expensive equipment that must be operated by qualified professionals in a safe environment. To overcome these difficulties, the lab-on-a-chip concept was introduced [4], which aims to reduce the costs of analysis using platforms made of miniaturized active materials supported on quartz, glass, or polymers [5]. Recently, paper-based analytical devices (PADs) have gained attention as an innovative alternative, taking advantage of the accessibility and affordability of paper, which is renewable and recyclable [6–8]. Furthermore, PADs are easy to store, transport, and handle, and could be printed or coated for many applications [9]. Their high surface area, compatibility with biomolecules, and excellent filtration properties make them suitable for lateral flow assays, chromatographic separations, and microfluidic devices. In addition, most PADs are biodegradable and can be disposed by incineration, making them environmentally friendly, biocompatible, and efficient tools that require minimal use of samples and reagents, while ensuring easy operation [9].

In recent decades, biosensors have attracted considerable interest in both the scientific and industrial sectors [10–15]. These devices cleverly integrate biology, physics, chemistry, and engineering knowledge, offering relevant and practical solutions to contemporary analytical challenges [10–15]. However, several studies have reported on biosensors based on MOF platforms for biomolecule immobilization, but only a few examples based on PADs have been explored [16–25]. Ortiz-Gómez et al. (2017) [18] developed a microfluidic paper-based analytical device (μPAD) for glucose determination using a supported MIL-101 (Fe) MOF acting as a peroxidase mimic, and under optimal conditions, the value for the S coordinate increases linearly for glucose concentrations up to 150 $\mu mol \cdot L^{-1}$, with a 2.5 $\mu mol \cdot L^{-1}$ detection limit. In that same sense, Wei et al. (2021) [19] reported an electrochemical sensor based on Co-MOF modified carbon cloth/paper applied to quantitative glucose detection, effectively increasing the specific area and catalytic sites more than a traditional plane electrode. Also, Hassanzadeh et al. (2019) [20] presented a luminescent PAD to estimate total phenolic content based on a H_2O_2−rhodamine b−Co-MOF. It was discovered that the reaction of H_2O_2 with rhodamine b molecules, loaded into the Co-MOF nanopores, can enhance their emission. Recently, Catalá-Icardo et al. (2024) [21] fabricated MIL-53 (Al)-modified PADs for the efficient extraction of neonicotinoid insecticides. The whole method showed satisfactory analytical performance with recoveries between 86 and 114%, suitable precision (with RSD lower than 14%), and detection limits ranging from 1 to 1.6 $\mu g \cdot L^{-1}$. Moreover, Chang et al. (2024) [22] proposed colorimetric PADs based on a two-dimensional MOF nanozyme for a dichlorophen assay. On the other hand, Feng et al. (2024) [23] reported a paper-based electrochemiluminescence biosensor for detecting pathogenic bacteria *Staphylococcus aureus*. This biosensor was constructed using porous Zn-MOFs to form $[Ru\ (bpy)_3]^{+2}$ functionalized MOF nanoflowers (MOF-5 (Ru) NFs) [23]. In addition, Guan et al. (2024) [24] fabricated a hydrogel-based colorimetric PADs platform for the visual colorimetric assay of creatinine using CdTe@UiO-66-PC-Cu MOF. Definitely, PAD biosensors based on MOF platforms for biomolecule immobilization open exciting doors for the development of analytical devices.

In the present research, we synthesized and characterized three amino-functionalized MOF platforms (UiO-66-NH_2 (Zr), MIL-125-NH_2 (Ti), and MIL-101-NH_2 (Fe)) and employed them to develop sensitive, portable PADs for monitoring ALP enzyme activity by laser-induced fluorescence.

2. Materials and Methods

2.1. Reagents and Materials

All of the used reagents were analytical grade and were purchased without further purification treatment. 2-aminoterephthalic acid (H_2ATA), methanol (MeOH), zirconium tetrachloride ($ZrCl_4$), titanium isopropoxide (Ti $(OiPr)_4$), N,N′-dimethylformamide (DMF), and 2-amino-1,4-benzenedicarboxylic acid were purchased from Merck (Darmstadt, Germany). Dopamine hydrochloride, Tris-HCl, and Iron (III) chloride hexahydrate ($FeCl_3 \cdot 6H_2O$, 97%) were purchased from J&K Scientific Ltd. (San José, CA, USA); 4-methylumbelliferyl phosphate (4-MUP) from Fluka and alkaline phosphatase (ALP) enzyme were purchased from Sigma-Aldrich (Buenos Aires, Argentina). Hydrogen peroxide (H_2O_2) 30% (v/v), glutaraldehyde (GLU, 5% aqueous solution), and acetone were purchased from Merck (Darmstadt, Germany). Filter paper N° 1 was provided by Whatman (Maidstone, UK). All buffer solutions were prepared with milli-Q water.

2.2. Equipment

An Orion Research Inc. model EA 940 equipped with a glass combination electrode (Orion Research 95 Inc., Cambridge, MA, USA) was employed for pH determinations. In addition, MOF platforms were characterized using an LEO 1450VP scanning electron microscope (SEM). A Xerox Color-Qube 8870 printer was used to mark the paper microzones. The fluorescent signal was monitored under LED excitation at 430 nm. All the samples were placed at 45 ° with respect to the LED beamline. The fluorescent radiation was detected with the assembly′s optical axis perpendicular to the device′s plane. A microscope objective (10:1, PZO, Poland) mounted on a BIOLAR L-PZO microscope was used for light collection. A fiber-optic collection bundle was mounted on a sealed housing at the end of the microscope lens, connected to an Ocean Optics model QE65000-FL spectrometer. In order to avoid spurious light, the entire assembly was covered with a large black box. The powder X-ray diffraction (PXRD) plots were recorded with a Rigaku—Ultima IV type II diffractometer. A scanning step of 0.05° between 5 and 50 2-theta Bragg angles with an exposure time of 5 s per step was used to obtain the best counting statistics. Fourier transform infrared (FTIR) spectroscopic measurements were obtained in a Perkin Elmer Spectrum 65 FTIR spectrometer in a region from 400 to 4000 cm^{-1}.

2.3. Synthesis of Amino-MOFs

The synthesis of MIL-125-NH_2 (Ti) was carried out following a previously reported procedure [10] with some modifications in the amounts of the components: 0.54 g of H_2ATA ($0.294 \cdot 10^{-3}$ mol·L^{-1}) and 0.315 mL of Ti$(OiPr)_4$ ($1.05 \cdot 10^{-3}$ mol·L^{-1}) were mixed in 24 mL of DMF solution and 6 mL of MeOH solution. The mixture was stirred for 30 min, then transferred to a 45 mL Parr reactor coated internally with Teflon and heated to 150 °C for 72 h. After that, a pale yellow powder was obtained. The solid underwent a two-step washing process with continuous stirring at 500 rpm: initially with 45 mL of a DMF solution, followed by 20 mL of an MeOH solution. Afterward, the solid was dried at 75 °C in an oven for 48 h (yield 48%). The resulting powder was reduced in particle size through manual grinding for 90 min in an agate mortar. Then, a 0.5% w/v suspension of MIL-125-NH_2 (Ti) in 0.1 mol·L^{-1} phosphate buffer solution (PBS) pH 7.2 was prepared and sonicated for 60 min. The UiO-66-NH_2 (Zr) synthesis was carried out following previously described steps [11] with some modifications in the amounts of the components: 0.288 g of anhydrous $ZrCl_4$ (1.23×10^{-3} mol·L^{-1}) and 0.209 g (1.92×10^{-3} mol·L^{-1}) of H_2ATA were dissolved in 60 mL of DMF and stirred for 30 min. Subsequently, the solution was transferred to a 45 mL Teflon-lined Parr reactor and brought to 120 °C for 24 h (yield 55%). After that, it was cooled to room temperature, and the resulting light brown powder was washed three times with DMF solution and finally dried at 70 °C for 24 h. A 0.1 mol·L^{-1} pH 7.2 PBS buffer solution containing 0.5% w/v of UiO-66-NH_2 (Zr) was prepared for analytical measurements. The synthesis of MIL-101-NH_2 (Fe) followed steps previously described [12], with some modifications. Masses of 0.504 g of anhydrous $FeCl_3 \cdot 6H_2O$

(2×10^{-3} mol·L^{-1}) and 0.181 g (1×10^{-3} mol·L^{-1}) of H_2ATA were mixed in 15 mL of DMF under constant stirring for 30 min. The mixture was transferred into a 120 mL stainless steel Parr autoclave reactor internally lined with Teflon, which was hermetically sealed and heated at 120 °C for 24 h. After cooling to room temperature, the resulting dark brown powder was washed with constant agitation using 20 mL of DMF for 24 h. Finally, the product was dried at 75 °C for 48 h (yield 19%). Before employing the product, a 0.1 mol·L^{-1} PBS buffer solution pH 7.2 containing 0.5% w/v of the MIL-101-NH_2 (Fe) was prepared.

2.4. Biosensor Design

Whatman No.1 filter paper was used to design and construct the immunosensor. A 6 mm diameter hydrophobic containment barrier was delimited circularly on a microzone of this paper by wax stamping, using Corel Draw 9 graphic software and the Xerox ColorQube 8870 wax printer. The cut papers were then placed on a hot plate at 80 °C to homogenize the walls forming the hydrophobic wax barrier.

The papers were subjected to a constant flow of oxygen plasma for 3 min to generate as many aldehyde groups as possible on their surface by cellulose oxidation, in order to have a more significant surface reaction.

2.5. Paper Modification

Suspensions of UiO-66-NH_2 (Zr), MIL-125-NH_2 (Ti), and MIL-101-NH_2 (Fe) were prepared at a concentration of 0.5% w/v in 0.1 mol·L^{-1} PBS buffer solution pH 7.2 and dispersed under sonication for 15 min. When the suspensions were completely homogenized, 20 µL was placed onto the pre-treated papers using a drop casting method and left in a humid chamber for 30 min. During this time, the aldehyde groups on the cellulose surface linked to the amino groups of the mentioned MOFs. After that, the papers were washed three times with 0.1 mol·L^{-1} PBS buffer solution pH 7.2 and dried under N_2 flow.

2.6. Enzyme Immobilization

To achieve covalent bonds between the amino groups of the immobilized MOFs on the paper with the amino groups present in the ALP, a cross-linking agent solution of glutaraldehyde (GLU) was employed. This procedure consisted of the following steps: First, the papers were immersed for 30 min in a 0.5% w/v GLU acetone solution at pH 8. After being washed three times with 0.1 mol·L^{-1} pH 7.2 PBS buffer solution and dried, 20 µL of 0.1% w/v ALP solution in 0.1 mol·L^{-1} PBS buffer solution pH 7.2 was added and incubated at 37 °C for 10 min. Subsequently, the papers were washed three times with PBS buffer solution to remove excess non-bounded protein (Figure 1).

2.7. Study of the Enzymatic Response by Laser-Induced Fluorescence

An optical system was constructed using a single frequency 430 nm DPSS laser (Cobolt Zouk^{TM}) operated at 10 mW that served as the fluorescence excitation source to detect enzyme activity and test the paper biosensor. The laser was focused on the detection channel at 90° geometry with respect to the surface.

The relative fluorescence signal, which corresponded to the ALP, was measured in situ on the modified paper device. The fluorescence of 4-MUP was measured using excitation at 430 nm and emission at 452 nm. Diethanolamine (DEA) buffer (0.1 mol·L^{-1} diethanolamine, 5×10^{-2} mol·L^{-1} KCl, 1×10^{-3} mol·L^{-1} $MgCl_2$, pH 9.6) was used to prepare the 4-MUP solution. Finally, 5 µL of substrate solution (2.5×10^{-3} mol·L^{-1} 4-MUP in DEA buffer solution, pH 9.6) was injected into the modified paper, and LIF was used to measure the enzyme product.

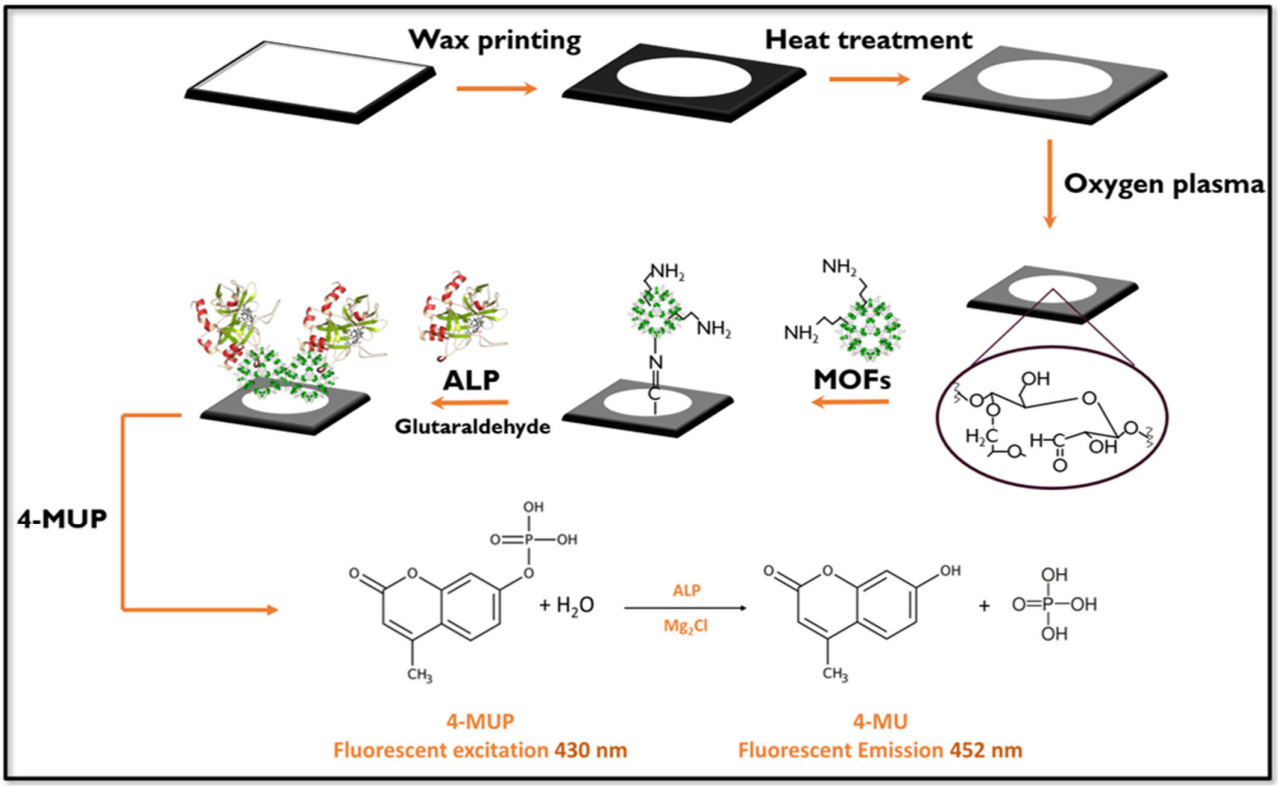

Figure 1. Schematic representation of fluorescent paper-based biosensor construction showing the modification of the paper surface and the alkaline phosphatase determination procedure.

The paths of the reflected beams were meticulously arranged to prevent collisions with other components of the device cell, thereby minimizing the risk of photobleaching. Fluorescent radiation was detected along the optical axis of the array. An optical fiber collection system was installed within a sealed housing linked to the QE65000-FL scientific-grade spectrophotometer (Ocean Optics, Inc., New York, NY, USA). The entire system was enclosed within a black box during measurements to eliminate spurious light interference. These assessments were conducted for both a blank assay where the enzyme was directly immobilized onto unmodified paper, and assays where the enzyme was immobilized onto papers modified with three amino-functionalized MOFs.

3. Results and Discussion

3.1. Elemental Characterization of MOFs

SEM–EDS

The synthesized MOFs were characterized by SEM and EDS analysis to obtain information regarding the particle size and semi-quantitative elemental percentage. As shown in Figure 2a, MIL-125-NH_2 (Ti) particles exhibit a spherical morphology with an average size of approximately 0.6 ± 0.2 µm. Moreover, the EDS data indicate the presence of high lines from titanium metal ions and signals from C and O belonging to the organic backbone (Figure 3a).

In Figure 2b, the particles of UiO-66-NH_2 (Zr) showed a flat morphology with an average size of 0.53 ± 0.2 µm, confirming the elemental composition of the metal Zr and the ligand components C and O (Figure 3b). Finally, besides Figure 2c, the MIL-101-NH_2 (Fe) particles exhibited a spherical shape with a uniform average size of 0.26 ± 0.06 µm. Also, EDS analysis revealed characteristic X-ray lines corresponding to the iron along with O and C from the ligands.

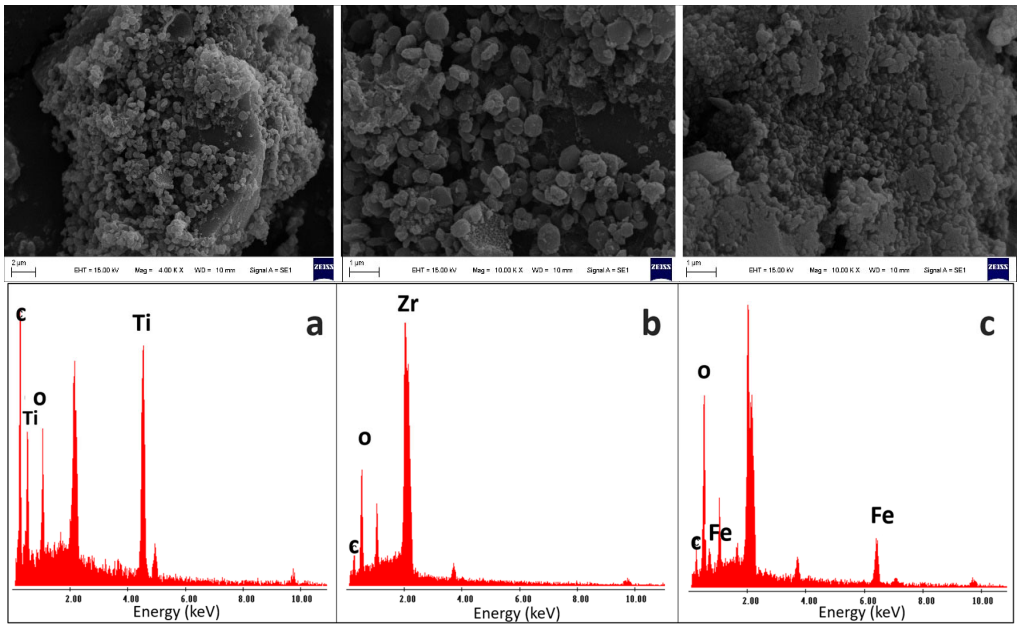

Figure 2. SEM image characterization: (**a**) MIL-125-NH_2 (Ti), (**b**) UiO-66-NH_2 (Zr), and (**c**) MIL-101-NH_2 (Fe).

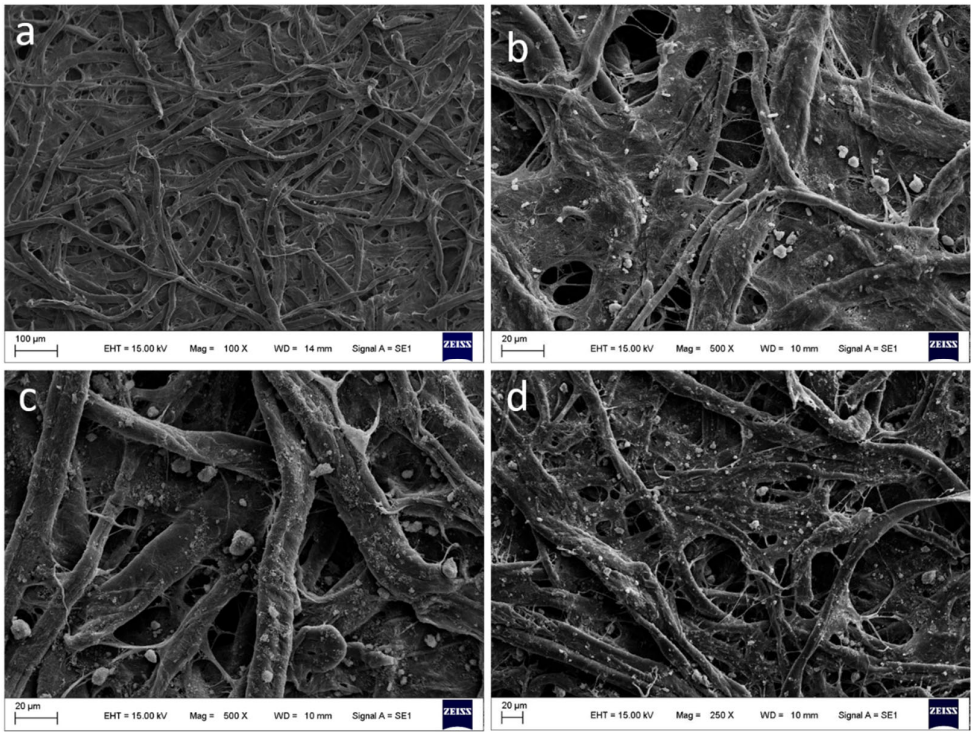

Figure 3. SEM image characterization: (**a**) unmodified paper surface, (**b**) paper surface modified with amino-functionalized MIL-101-NH_2 (Fe), (**c**) paper surface modified with amino-functionalized UiO-66-NH_2 (Zr), and (**d**) paper surface modified with amino-functionalized MIL-125-NH_2 (Ti).

The paper supports, with and without modifications, were also characterized by SEM and EDS techniques, as illustrated in Figures 3 and 4. In the unmodified paper, the cellulose fibers are shown in their original state provided by the manufacturer, with characteristic EDS peaks confirming their C and O composition (see Figure 4a). Figure 3b shows the impregnated paper with MIL-101-NH_2 (Fe), revealing visible particles deposited on the support and confirming this observation through an X-ray line spectrum (see Figure 4b).

In Figure 3c, the MOF UiO-66-NH_2 (Zr) is observed impregnating the cellulose support, with visible particles deposited and elemental composition that confirms the presence of cellulose and mesoporous elements (see Figure 4c). Finally, Figure 3d shows cellulose paper impregnated with MIL-125-NH_2 (Ti), demonstrating the presence of elements through composition analysis (see Figure 4c) and a uniform dispersion of particles throughout the paper.

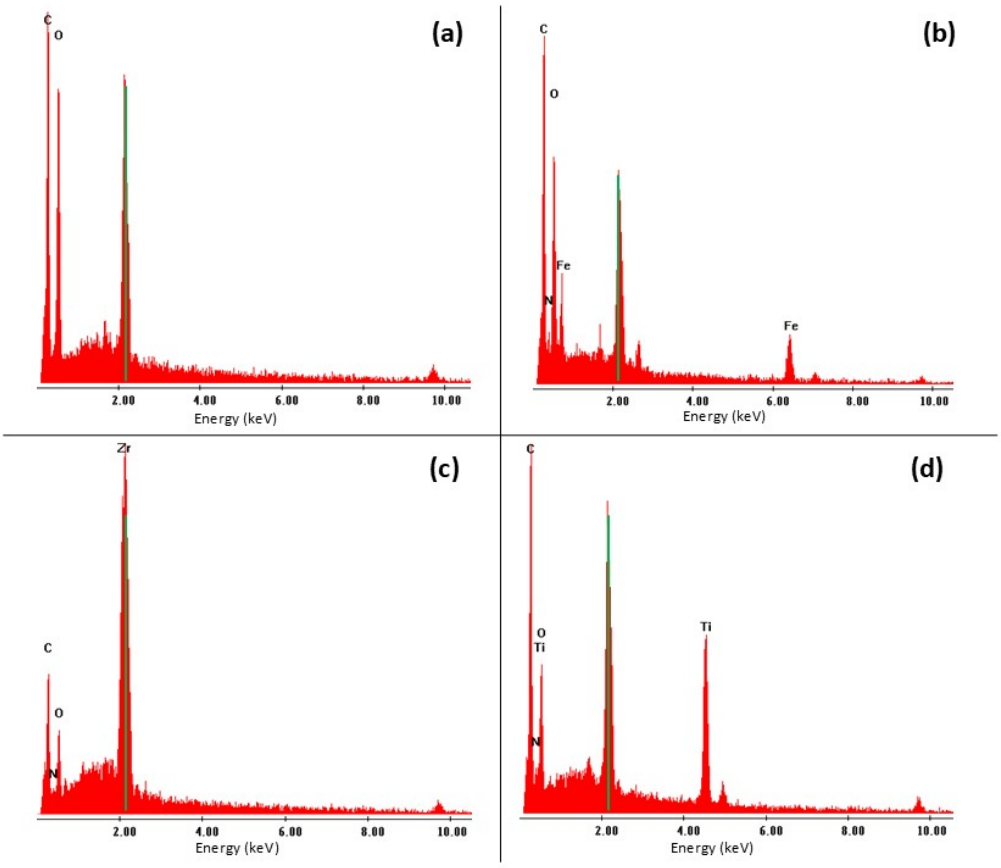

Figure 4. EDS spectra characterization: (**a**) unmodified paper surface, (**b**) paper surface modified with amino-functionalized MIL-101-NH_2 (Fe), (**c**) paper surface modified with amino-functionalized UiO-66-NH_2 (Zr), and (**d**) paper surface modified with amino-functionalized MIL-125-NH_2 (Ti). Note: the peak centered at 2.12 keV corresponds to the sputtered gold employed for the SEM technique.

3.2. Powder X-ray Diffraction (PXRD)

Using powder PXRD, experimental diffractograms were compared with the corresponding simulated powder plots (the latter were obtained using cif files extracted from the literature [10–12]). In MIL-101-NH_2 (Fe), the presence of a single phase could be verified. However, lower intensities are observed in the diffraction peaks, possibly due to a lower crystallinity related to the synthesis method (see Figure 5a). This MOF crystallized in the cubic space group Fd-3 m (No. 227). Performing the same analysis for the UiO-66-NH_2 (Zr) phase, a coincidence is also observed between the experimental pattern and its corresponding theoretical one (see Figure 5b). The compound with the formula crystallized in the cubic space group Fm-3 m. Figure 5c shows the comparison between the theoretical and experimental diffractograms of MIL-125-NH_2 (Ti), concluding in a broad coincidence between the diffraction peaks, confirming the presence of a single pure phase. This MOF was indeed found to be crystallized in the orthorhombic space group I4/mmm (N° 139).

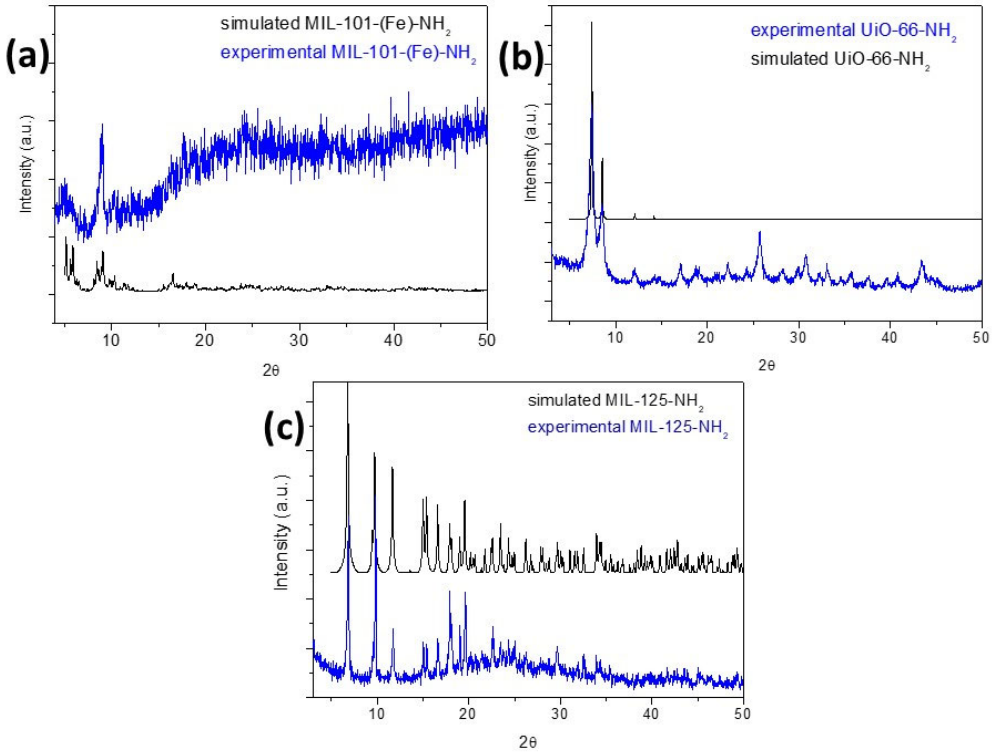

Figure 5. Experimental PXRD patterns of (**a**) MIL-101-NH_2 (Fe), (**b**) UiO-66-NH_2 (Zr), and (**c**) MIL-125-NH_2 (Ti) (blue lines) compared to the simulated diffractograms.

MIL-101-NH_2-Fe, with composition {[Fe_3 (μ_3-O) (μ4-2-ATA)$_3$ $(H_2O)_2Cl$]}, belongs to the family of materials known as MIL-101 (where MIL stands for Matériaux de l'Institut Lavoisier) [25]. The crystal structure of MIL-101 (Fe)-NH_2 is composed of 2-ATA linkers and Fe (III) ions, which serve as metallic nodes. The Fe (III) ions form a trigonal planar cluster and a trigonal prismatic secondary building unit (see Figure 6a) [26]. Four of these building units are connected through six 2-ATA linkers, forming a supertetrahedral unit. Figure 6b shows the final crystal structure of MIL-101-NH_2 (Fe), which contains different cages and sizes: a microporous cage with entrance windows approximately 8.6 Å in free diameter, and two mesoporous cages with diameters of approximately 29 Å and 34 Å.

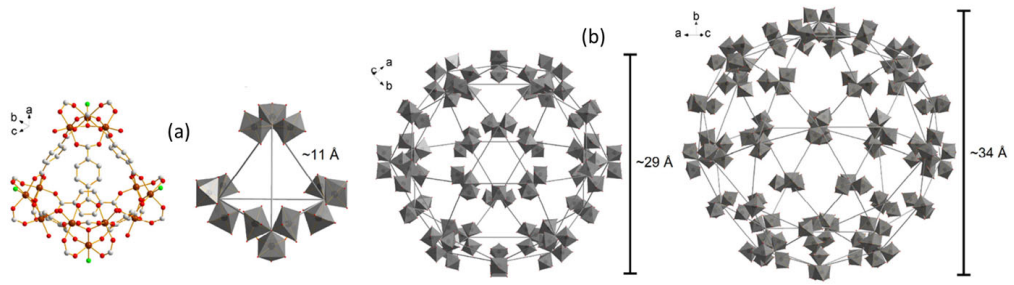

Figure 6. (**a**) Secondary building unit (color codes: gray: carbon; red: oxygen; green: chloride, brown: iron) and (**b**) the formed cages in MIL-101-NH_2 (Fe).

Figure 7 shows the most stable form of UiO-66-NH_2 (Zr), which consists of a face-centered-cubic structure containing an fm−3m symmetry with a lattice parameter of 20.7 Å. Moreover, it contains two separate cages, a tetrahedron cage of 7.5 Å, another octahedron cage of 12 Å, and a pore aperture of 6 Å [27].

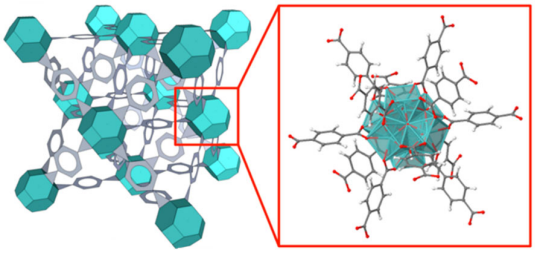

Figure 7. A schematic structure of UiO-66-NH_2 (Zr). The face-center-cubic UiO-66 structure type is composed of the metal node (aqua) and ligand (gray) with an atomic representation of the node and 12-connected 2-ATA linkers.

MIL-125-NH_2 (Ti) comprises [$Ti_8O_8(OH)_4$-(2-ATA)$_6$] building units, and its crystal structure is established from the cyclic octamers constructed from octahedral titanium units present at the edge or corner [28]. Also, these octamers are associated with 12 other cyclic octamers, giving rise to a porous 3-D quasi-cubic tetragonal structure (see Figure 8). Also, the structure has two types of cages, an octahedral (12.5 Å) and a tetrahedral (6 Å) cage, accessible through narrow triangular windows of ca. 6 Å.

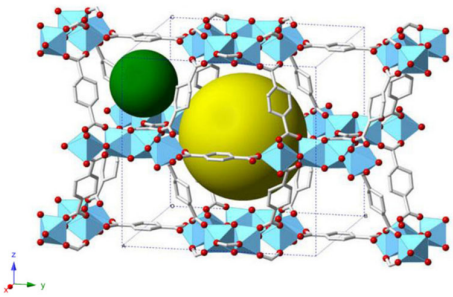

Figure 8. A schematic structure of MIL-125-NH_2-(Ti) (color codes: gray bars: carbon backnone; red: oxygen; light-blue polyhedra: titanium centers) shows the two cage types (green and yellow spheres).

3.3. Characterization of ALP Immobilization on the Support

FTIR

Another method employed to confirm the immobilization processes conducted on the paper substrate was Fourier transform infrared (FTIR) characterization.

The spectra provided below (see Figure 9) depict a comparison between the unaltered paper (shown in blue spectra) and the same paper modified with MIL-125-NH_2 (Ti), UiO-66-NH_2 (Zr), and MIL-101-NH_2 (Fe)—(black traces), followed by the subsequent stage where glutaraldehyde molecules were attached, leaving exposed terminal aldehyde groups (depicted in red spectra) for all three cases.

By the FTIR technique, it is possible to analyze the principal vibrational modes of the cellulose fibers and their interactions with the MOF particles. The paper exhibits the C-H stretching modes of cellulose located at 2850 cm^{-1} and a prominent band attributed to the vibrations of the C-O-C groups within the β-glucopyranose ring of cellulose at 1066 cm^{-1}. This band decreases significantly upon modifying the paper with MOFs, suggesting a robust covalent interaction between these bonds and the amino groups functionalizing the materials [9]. The following chemical reaction illustrates the bonding between the amino groups of MOFs and the aldehyde groups of cellulose.

$$\text{MOF-NH}_2 + \text{H-(CO)-C}_3\text{H}_6\text{-(CO)-H} \rightarrow \text{MOF-N=CH-C}_3\text{H}_6\text{-(CO)-H}$$

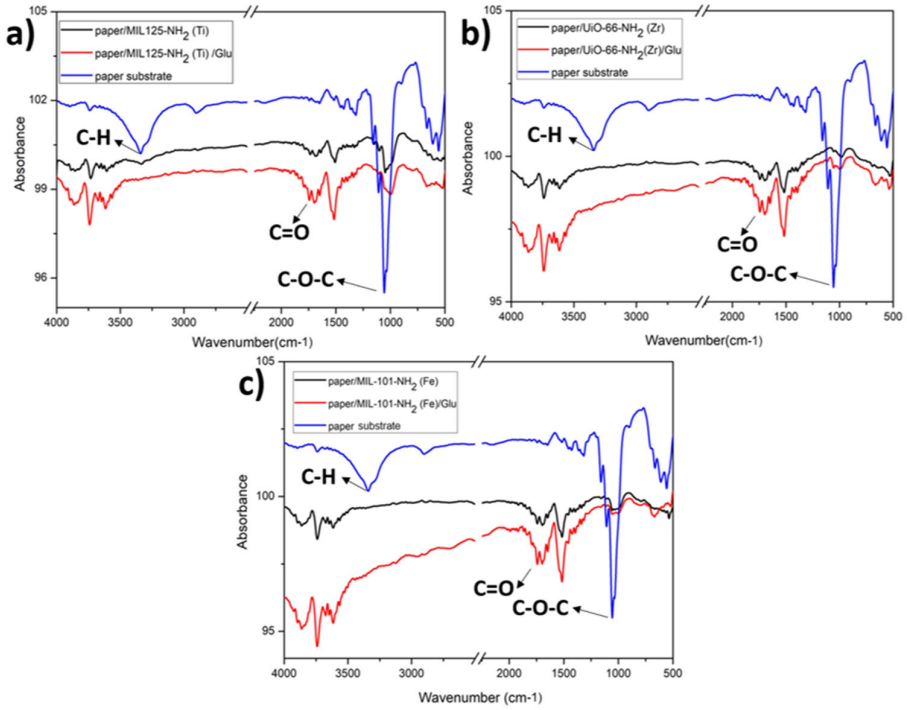

Figure 9. FTIR study of paper modification with (**a**) MIL-125-NH_2 (Ti) and subsequent stage with GLU; (**b**) UiO-66-NH_2 (Zr) and subsequent stage with GLU; and (**c**) MIL-101-NH_2 (Fe) and subsequent stage with GLU.

In all cases where the paper support is modified with different MOFs, the presence of solvent trapped in its pores is evident at 3625 cm^{-1}. Finally, there is an increase in the intensity of the carbonyl band (C=O stretching) centered at 1745 cm^{-1} when glutaraldehyde is bound to the MOFs.

3.4. Optimization of Experimental Parameters

To carry out the elemental parameter optimization tests, the following considerations were taken into account: adjust the MOF concentration for the paper support modification, adjust the ALP enzyme concentration, optimize the 4-MUP substrate concentration, determine the reaction time, and identify the optimum pH for enzymatic activity.

For the ALP enzyme, the substrate used was 4-MUP. After enzymatic action, the substrate produces 4-methylumbelliferone (4-MU), a fluorescent compound emitting at 452 nm.

In addition, to optimize the concentrations of the different MOFs used to modify the paper support, dispersions of the three MOFs were prepared in 1 mol·L^{-1} PBS buffer solution pH 7.2, in a concentration range of 0 to 0.8% w/v. The ALP enzyme was immobilized at 0.1% w/v in 0.1 mol·L^{-1} PBS buffer pH 7.2 for each modified paper with the different MOF concentrations. Finally, the ALP response was monitored using 5 µL of fluorescent substrate solution (2.5×10^{-3} mol·L^{-1} 4-MUP in DEA buffer solution (0.1 mol·L^{-1} diethanolamine, 5×10^{-2} mol·L^{-1} KCl, 1×10^{-3} mol·L^{-1} $MgCl_2$) pH 9.6) in each paper microzone. Subsequently, the enzyme product was measured using LIF.

The obtained signal from the enzymatic response was greater when the microzones of the paper were modified with different concentrations of MIL-125-NH_2 (Ti), which demonstrates that there is an increase in the immobilization surface due to the incorporation of MIL-125-NH_2 (Ti) in comparison to UiO-66-NH_2 (Zr) and MIL-101-NH_2 (Fe). On the other hand, when higher concentrations of MIL-125-NH_2 (Ti) than 0.5% w/v were used, a system saturation was observed, so this was selected as the concentration limit for all subsequent tests (see Figure 10).

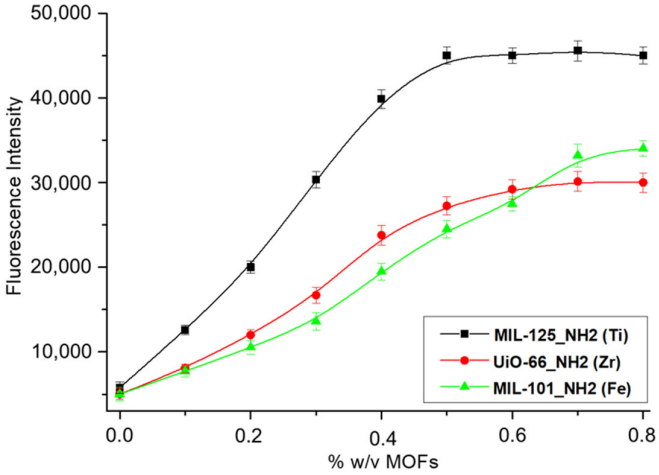

Figure 10. Optimization of impregnated MOF concentrations for paper support modification.

In light of these results highlighting the differential response of the modified papers with MIL-125-NH_2 (Ti)/ALP compared to those with UiO-66-NH_2 (Zr)/ALP, MIL-101-NH_2 (Fe)/ALP, it was decided to continue with the optimizations of experimental variables using the MOF MIL-125-NH_2 (Ti) as a proposal for the best surface to apply to the development of biosensors.

According to the literature, MIL-101-NH_2 (Fe) exhibits a higher BET surface area of 3528 $m^2 \cdot g^{-1}$ and a pore volume of 1.48 $cm^3 \cdot g^{-1}$ [26] with respect to those values from MIL-125-NH_2 (Ti) (1469 $m^2 \cdot g^{-1}$ and a pore volume of 0.6 $cm^3 \cdot g^{-1}$) [28] and UiO-66-NH_2 (Zr) (822 $m^2 \cdot g^{-1}$ and a pore volume of 0.23 $cm^3 \cdot g^{-1}$) [29]. Nevertheless, MIL-125-NH_2 (Ti) exhibits better immobilization performance, which could be reasonably attributed to a lower pore volume and, consequently, lower water occupancy.

Optimizing the concentration of ALP employed for immobilization was a critical parameter to evaluate. Therefore, a comprehensive study was conducted within the 0.1 to 2.5 $mg \cdot mL^{-1}$ concentration range. Figure 11a illustrates that the fluorescence intensity increased proportionally with the concentration of immobilized ALP, reaching a peak at 1 $mg \cdot mL^{-1}$. Beyond this concentration, the intensity plateaued, indicating saturation. Consequently, 1 $mg \cdot mL^{-1}$ of ALP emerged as the optimal concentration for immobilization on modified paper with 0.5% w/v of MIL-125-NH_2 (Ti) suspension.

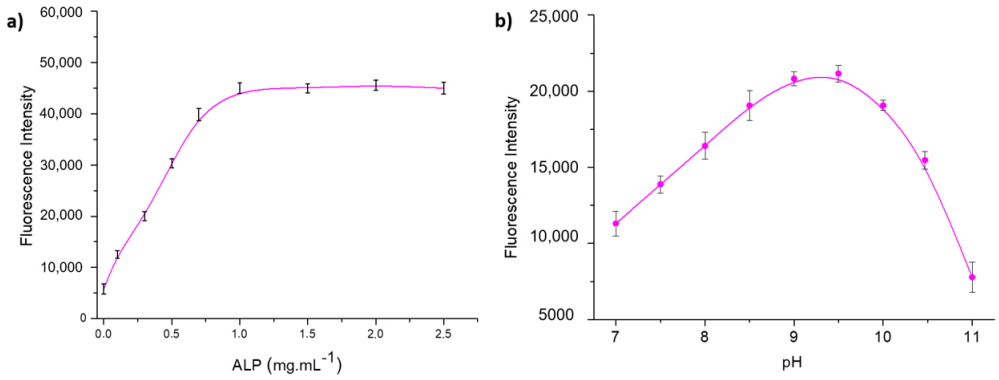

Figure 11. (**a**) Optimization of the ALP concentration used for immobilization; (**b**) optimization of the optimal pH range of the enzymatic activity.

The impact of pH on the enzymatic response was also evaluated by adjusting the pH of the substrate solution to a range of 7 to 11. The enzyme activity exhibited its maximum value when the DEA buffer solution was at a pH of 9.6, as shown in Figure 11b. Therefore, pH 9.6 was selected as the optimal pH for all subsequent experimental measurements.

The impact of 4-MUP concentration on the enzymatic response of ALP was investigated within the range of 0.1×10^{-3}–5.0×10^{-3} mol·L^{-1} in DEA buffer solution at pH 9.6. The optimal concentration of 4-MUP, which produces the highest enzymatic response, was determined to be 2.5×10^{-3} mol·L^{-1}, as shown in Figure 12a. As a consequence, this concentration was adopted for all subsequent experimental measurements.

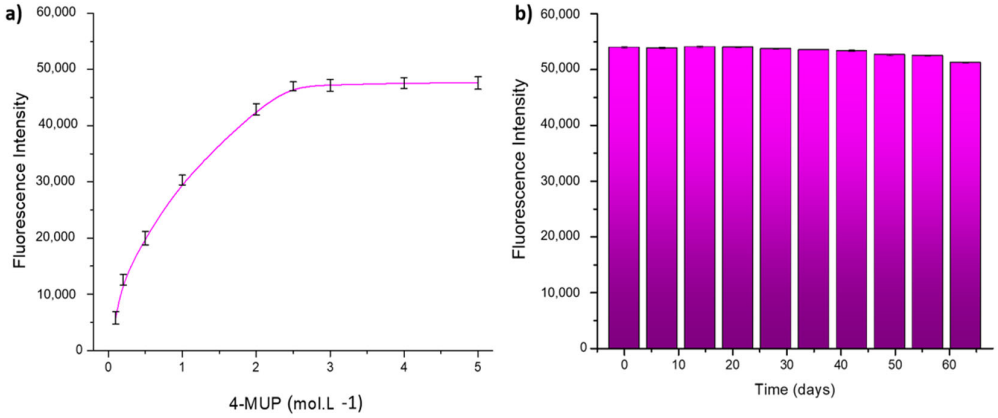

Figure 12. (**a**) Optimization of 4-MUP concentration; (**b**) stability tests of the modified paper support.

Long-term stability testing of the system was performed by freeze-drying the MIL-125-NH_2 (Ti)/ALP-modified paper devices and storing them at 4 °C, protected from light. Measurements were taken every 7 days, as illustrated in Figure 12b. In particular, the fluorescent signal response remained practically constant after 45 days, with only a 5% decrease observed after 60 days. This result shows the reproducibility of the sensor signal.

Reaction time is also a crucial parameter to define, especially in applications that demand fast and reliable analysis. This study used MIL-125-NH_2 (Ti)/ALP/4-MUP-modified papers and analyzed them at various incubation times ranging from 20 to 240 s. The fluorescence intensity progressively increased with longer incubation periods until reaching 180 s. Beyond this point, a saturation effect became evident. Consequently, the optimal reaction time was determined to be 180 s (see Figure 13). Finally, a summary of the experimental working experiments is depicted in Table 1.

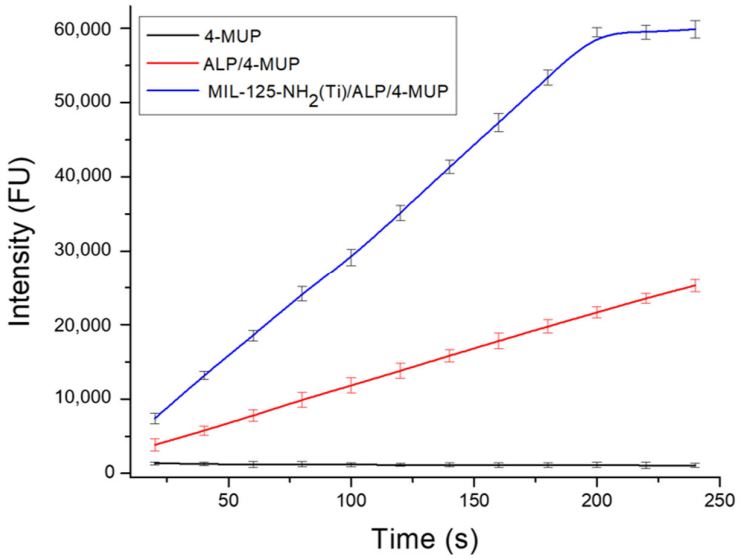

Figure 13. Fluorescence response at different incubation times of MIL-125-NH_2 (Ti)/ALP/4-MUP by modifying the paper support.

Table 1. Summary of optimal working conditions.

Sequence	Condition	Time (min)/Temperature (°C)
Cellulose oxidation	Oxygen plasma	3/room temperature
Modification of paper	0.5% w/v MOFs suspensions in PBS buffer solution, pH 7.2	30/room temperature in wet chamber
Washing buffer	PBS buffer solution, pH 7.2	1 min at a time
Cross-linking	0.5% w/v GLA in acetone pH 8	30/room temperature
Washing buffer	PBS buffer solution, pH 7.2	1 min at a time
Enzyme	1 mg.mL^{-1} ALP in PBS buffer solution pH 7.2	10/37 °C
Washing buffer	PBS buffer solution, pH 7.2	1 min at a time
Substrate	2.5×10^{-3} mol.L^{-1} 4-MUP in DEA buffer solution, pH 9.6	2

4. Conclusions

In our research, MIL-125-NH_2 (Ti), UiO-66-NH_2 (Zr), and MIL-101-NH_2 (Fe) MOFs were synthesized, characterized, and successfully used for the modification of paper surfaces towards development of PADs biosensors. It could be concluded that the MIL-125-NH_2 (Ti) MOF significantly increased the effective surface area for the immobilization of biomolecules in comparison to UiO-66-NH_2 (Zr) and MIL-101-NH_2 (Fe). This feature was confirmed by immobilizing the ALP enzyme and monitoring its activity by laser-induced fluorescence, giving rise to a higher signal intensity for the same concentrations of the three dispersions and modifying the paper support. In the light of these features, we chose MIL-125-NH_2 (Ti) for further optimization trials to conclude a reliable and reproducible platform suitable for biomolecule detection. Consequently, the MIL-125-NH_2(Ti)/ALP-modified papers showed excellent stability and reproducibility, demonstrating the potential use of this new modified platform for developing biosensors for the rapid detection of various bioanalytes of interest.

Author Contributions: Conceptualization, S.V.P., G.E.G. and M.A.F.-B.; methodology, S.V.P., G.E.G., and M.A.F.-B.; validation, S.V.P., G.R.T., A.B.S., M.D.R. and G.A.M.; formal analysis, S.V.P., G.E.G., M.D.R. and M.A.F.-B.; resources, S.V.P., G.R.T., A.B.S., M.D.R. and G.A.M.; writing—original draft preparation, S.V.P., G.E.G. and M.A.F.-B.; writing—review and editing, S.V.P., G.E.G., G.R.T., A.B.S., G.A.M. and M.A.F.-B.; supervision, G.E.G. and M.A.F.-B.; project administration, G.E.G., G.A.M. and M.A.F.-B.; funding acquisition, G.A.M. and M.A.F.-B. All authors have read and agreed to the published version of the manuscript.

Funding: Funding is acknowledged from the Universidad Nacional de San Luis (PROICO 02-2220), from Agencia Nacional de Promoción Científica y Tecnológica (AGENCIA, FONCyT, Argentina, PICT-2021-GRF-TII-0390, PICT-2021-GRF-TI-0136, PICT-2020-2347, and PICT-2020-2369), from Consejo Nacional de Investigaciones Científicas y Técnicas (CONICET, Argentina, PIP11220200100033CO), from Ministerio de Ciencia, Tecnología e Innovación, Argentina, Proyectos de Redes Federales de Alto Impacto: NANOQUIMISENS (IF-2023-85161983-APN-DNOYPI#MCT), and from Agencia Nacional de Investigación y Desarrollo (ANID) (ANID/FOVI220003).

Institutional Review Board Statement: Not applicable.

Informed Consent Statement: Not applicable.

Data Availability Statement: The complete data of this study can be obtained upon request from the corresponding author.

Acknowledgments: This research was supported by Universidad Nacional de San Luis, Instituto de Química de San Luis (INQUISAL); Consejo Nacional de Investigaciones Científicas y Técnicas (CONICET); and Agencia Nacional de Promoción Científica y Tecnológica (FONCYT) (PICT-BID).

Conflicts of Interest: The authors declare no conflicts of interest.

References

1. Batten, S.R.; Champness, N.R.; Chen, X.M.; Garcia-Martinez, J.; Kitagawa, S.; Öhrström, L.; O'Keeffe, M.; Suh, M.P.; Reedijk, J. Terminology of Metal-Organic Frameworks and Coordination Polymers (IUPAC Recommendations 2013). *Pure Appl. Chem.* **2013**, *85*, 1715–1724. [CrossRef]
2. Long, J.R.; Yaghi, O.M. The Pervasive Chemistry of Metal-Organic Frameworks. *Chem. Soc. Rev.* **2009**, *38*, 1213–1214. [CrossRef]
3. Xu, Q.; Kitagawa, H. MOFs: New Useful Materials—A Special Issue in Honor of Prof. Susumu Kitagawa. *Adv. Mater.* **2018**, *30*, 1803613. [CrossRef]
4. Figeys, D.; Pinto, D. Lab-on-a-Chip: A Revolution in Biological and Medical Sciences. *Anal. Chem.* **2000**, *72*, 330–335. [CrossRef]
5. Lu, R.; Shi, W.; Jiang, L.; Qin, J.; Lin, B. Rapid Prototyping of Paper-Based Microfluidics with Wax for Low-Cost, Portable Bioassay. *Electrophoresis* **2009**, *30*, 1497–1500. [CrossRef] [PubMed]
6. Cate, D.M.; Adkins, J.A.; Mettakoonpitak, J.; Henry, C.S. Recent Developments in Paper-Based Microfluidic Devices. *Anal. Chem.* **2015**, *87*, 19–41. [CrossRef]
7. Martinez, A.W.; Phillips, S.T.; Whitesides, G.M.; Carrilho, E. Diagnostics for the Developing World: Microfluidic Paper-Based Analytical Devices. *Anal. Chem.* **2010**, *82*, 3–10. [CrossRef] [PubMed]
8. Wang, S.; Ge, L.; Song, X.; Yan, M.; Ge, S.; Yu, J.; Zeng, F. Simple and Covalent Fabrication of a Paper Device and Its Application in Sensitive Chemiluminescence Immunoassay. *Analyst* **2012**, *137*, 3821–3827. [CrossRef]
9. Pelton, R. Bioactive Paper Provides a Low-Cost Platform for Diagnostics. *TrAC Trends Anal. Chem.* **2009**, *28*, 925–942. [CrossRef]
10. Hendon, C.H.; Tiana, D.; Fontecave, M.; Sanchez, C.; D'Arras, L.; Sassoye, C.; Rozes, L.; Mellot-Draznieks, C.; Walsh, A. Engineering the Optical Response of the Titanium-MIL-125 Metal-Organic Framework through Ligand Functionalization. *J. Am. Chem. Soc.* **2013**, *135*, 10942–10945. [CrossRef]
11. Ding, L.; Shao, P.; Luo, Y.; Yin, X.; Yu, S.; Fang, L.; Yang, L.; Yang, J.; Luo, X. Functionalization of UiO-66-NH_2 with Rhodanine via Amidation: Towarding a Robust Adsorbent with Dual Coordination Sites for Selective Capture of Ag (I) from Wastewater. *Chem. Eng. J.* **2020**, *382*, 123009. [CrossRef]
12. Shan, Y.; Xu, C.; Zhang, H.; Chen, H.; Bilal, M.; Niu, S.; Cao, L.; Huang, Q. Polydopamine-Modified Metal–Organic Frameworks, NH_2-Fe-MIL-101, as PH-Sensitive Nanocarriers for Controlled Pesticide Release. *Nanomaterials* **2020**, *10*, 2000. [CrossRef] [PubMed]
13. Pashazadeh-Panahi, P.; Belali, S.; Sohrabi, H.; Oroojalian, F.; Hashemzaei, M.; Mokhtarzadeh, A.; de la Guardia, M. Metal-Organic Frameworks Conjugated with Biomolecules as Efficient Platforms for Development of Biosensors. *TrAC Trends Anal. Chem.* **2021**, *141*, 116285. [CrossRef]
14. Sohrabi, H.; Salahshour Sani, P.; Orooji, Y.; Majidi, M.R.; Yoon, Y.; Khataee, A. MOF-Based Sensor Platforms for Rapid Detection of Pesticides to Maintain Food Quality and Safety. *Food Chem. Toxicol.* **2022**, *165*, 113176. [CrossRef]
15. Osman, D.I.; El-Sheikh, S.M.; Sheta, S.M.; Ali, O.I.; Salem, A.M.; Shousha, W.G.; EL-Khamisy, S.F.; Shawky, S.M. Nucleic Acids Biosensors Based on Metal-Organic Framework (MOF): Paving the Way to Clinical Laboratory Diagnosis. *Biosens. Bioelectron.* **2019**, *141*, 111451. [CrossRef]
16. Dai, C.; Gan, Y.; Qin, J.; Ma, L.; Liu, Q.; Huang, L.; Yang, Z.; Zang, G.; Zhu, S. An Ultrasensitive Solid-State ECL Biosensor Based on Synergistic Effect between Zn-NGQDs and Porphyrin-Based MOF as "on-off-on" platform. *Colloids Surf. B Biointerfaces* **2023**, *226*, 113322. [CrossRef] [PubMed]
17. Li, M.; Zhang, G.; Boakye, A.; Chai, H.; Qu, L.; Zhang, X. Recent Advances in Metal-Organic Framework-Based Electrochemical Biosensing Applications. *Front. Bioeng. Biotechnol.* **2021**, *9*, 797067. [CrossRef]
18. Ortiz-Gómez, I.; Salinas-Castillo, A.; García, A.G.; Álvarez-Bermejo, J.A.; de Orbe-Payá, I.; Rodríguez-Diéguez, A.; Capitán-Vallvey, L.F. Microfluidic Paper-Based Device for Colorimetric Determination of Glucose Based on a Metal-Organic Framework Acting as Peroxidase Mimetic. *Microchim. Acta* **2018**, *185*, 47. [CrossRef]
19. Wei, X.; Guo, J.; Lian, H.; Sun, X.; Liu, B. Cobalt Metal-Organic Framework Modified Carbon Cloth/Paper Hybrid Electrochemical Button-Sensor for Nonenzymatic Glucose Diagnostics. *Sens. Actuators B Chem.* **2021**, *329*, 129205. [CrossRef]
20. Hassanzadeh, J.; Al Lawati, H.A.J.; Al Lawati, I. Metal-Organic Framework Loaded by Rhodamine b as a Novel Chemiluminescence System for the Paper-Based Analytical Devices and Its Application for Total Phenolic Content Determination in Food Samples. *Anal. Chem.* **2019**, *91*, 10631–10639. [CrossRef]
21. Catalá-Icardo, M.; Gómez-Benito, C.; Martínez-Pérez-Cejuela, H.; Simó-Alfonso, E.F.; Herrero-Martínez, J.M. Green Synthesis of MIL53 (Al)-Modified Paper-Based Analytical Device for Efficient Extraction of Neonicotinoid Insecticides from Environmental Water Samples. *Anal. Chim. Acta* **2024**, *1316*, 342841. [CrossRef] [PubMed]
22. Chang, J.; Hu, R.; Zhang, J.; Hou, T.; Li, F. Two-dimensional metal-organic framework nanozyme-mediated portable paper-based analytical device for dichlorophen assay. *Biosens. Bioelectron.* **2024**, *255*, 116271. [CrossRef] [PubMed]
23. Feng, Q.; Wang, C.; Miao, X.; Wu, M. A novel paper-based electrochemiluminescence biosensor for non-destructive detection of pathogenic bacteria in real samples. *Talanta* **2024**, *267*, 125224. [CrossRef] [PubMed]
24. Guan, J.; Xiong, Y.; Wang, M.; Liu, Q.; Chen, X. A novel functionalized CdTe@MOFs based fluorometric and colorimetric biosensor for dual-readout assay of creatinine. *Sens. Actuators B Chem.* **2024**, *399*, 134842. [CrossRef]
25. Lebedev, O.I.; Millange, F.; Serre, C.; Van Tendeloo, G.; Férey, G. First direct imaging of giant pores of the metal−organic framework MIL-101. *Chem. Mater.* **2005**, *17*, 6525–6527. [CrossRef]

26. Capková, D.; Almáši, M.; Kazda, T.; Čech, O.; Király, N.; Čudek, P.; Fedorková, A.S.; Hornebecq, V. Metal-organic framework MIL-101 (Fe)–NH_2 as an efficient host for sulphur storage in long-cycle Li–S batteries. *Electrochim. Acta* **2020**, *354*, 136640. [CrossRef]
27. Winarta, J.; Shan, B.; Mcintyre, S.M.; Ye, L.; Wang, C.; Liu, J.; Mu, B. A decade of UiO-66 research: A historic review of dynamic structure, synthesis mechanisms, and characterization techniques of an archetypal metal–organic framework. *Cryst. Growth Des.* **2019**, *20*, 1347–1362. [CrossRef]
28. Kim, S.-N.; Kim, J.; Kim, H.-Y.; Cho, H.-Y.; Ahn, W.-S. Adsorption/catalytic properties of MIL-125 and NH_2-MIL-125. *Catal. Today* **2013**, *204*, 85–93. [CrossRef]
29. Cao, Y.; Zhang, H.; Song, F.; Huang, T.; Ji, J.; Zhong, Q.; Chu, W.; Xu, Q. UiO-66-NH_2/GO composite: Synthesis, characterization and CO_2 adsorption performance. *Materials* **2018**, *11*, 589. [CrossRef]

Disclaimer/Publisher's Note: The statements, opinions and data contained in all publications are solely those of the individual author(s) and contributor(s) and not of MDPI and/or the editor(s). MDPI and/or the editor(s) disclaim responsibility for any injury to people or property resulting from any ideas, methods, instructions or products referred to in the content.